The mechanism of the amidases: Mutating the second active site glutamate inactivates the enzyme due to substrate mispositioning*

Brandon W. Weber[1], Serah W. Kimani[1,2], Arvind Varsani[1,3,4], Donald A. Cowan[5,6] Roger Hunter[7] Gerhard A. Venter[7] and B. Trevor Sewell[1,8]

[1]Structural Biology Research Unit, Division of Medical Biochemistry, Department of Clinical Laboratory Sciences, University of Cape Town, Observatory, Western Cape, 7700, South Africa

[2] Department of Molecular and Cell Biology, University of Cape Town, University Avenue, Rondebosch, Western Cape, 7700, South Africa

[3]School of Biological Sciences, University of Canterbury, Private Bag 4800,Christchurch 8140, New Zealand

[4]Biomolecular Interaction Centre, University of Canterbury, Private Bag 4800,Christchurch 8140, New Zealand

[5]Institute for Microbial Biotechnology and Metagenomics, Department of Biotechnology, University of the Western Cape, Bellville 7535 Cape Town South Africa

[6]Department of Genetics, University of Pretoria, Pretoria 0002, South Africa

[7]Scientific Computing Research Unit, Department of Chemistry, University of Cape Town, Rondebosch

[8]Institute of Infectious Diseases and Molecular Medicine, University of Cape Town, Observatory, Western Cape, 7700, South Africa

*Running title: *Mutating the second glutamate in the amidase active site*

To whom correspondence should be addressed: B. Trevor Sewell, Structural Biology Research Unit, Department of Clinical Laboratory Sciences, Institute of Infectious Diseases and Molecular Medicine, University of Cape Town, Observatory, Western Cape, 7700, South Africa, Tel.: +2721 650 2817; Fax: +2721 689 1528; Email: Trevor.Sewell@uct.ac.za

Keywords: amidase mechanism, catalytic tetrad, Michael adduct, acrylamide

Background: Amidases have a catalytic triad comprising a cysteine, a glutamic acid and a lysine.
Results: Mutating a neighbouring, structurally, conserved glutamic acid inactivates the enzyme. The mutated enzyme forms a Michael adduct with acrylamide.
Conclusion: The second glutamate is an essential catalytic residue which enables substrate positioning as one of its roles.
Significance: The amidases require an intact catalytic tetrad for activity.

SUMMARY

All known nitrilase superfamily amidase and carbamoylase structures have a second glutamate hydrogen bonded to the widely recognized catalytic lysine. Mutating this glutamate (E142) to a leucine in the amidase from *Geobacillus pallidus* renders the enzyme inactive. X-ray crystal structure determination shows that the structural integrity of the enzyme is maintained in spite of the mutation, with the catalytic cysteine (C166), lysine (K134) and glutamate (E59) in identical positions to those of the wild-type enzyme. The structural integrity is maintained in part by a chloride ion that is located in the position occupied by E142 $O^{\varepsilon 1}$ in the wild-type enzyme and thus interacts with the active site lysine. The active site cysteine of the mutated enzyme was found to form a Michael adduct with acrylamide, which is a substrate of the wild-type enzyme. The crystal structure of the adduct shows that the amide moiety interacts with the active site in a different manner than it does in the wild-type enzyme. The result is that the double bond of the acrylamide rather than the amide carbonyl carbon is adjacent to the active site cysteine. This demonstrates the role of the hydrogen bond between E142 $O^{\varepsilon 2}$ and the substrate amino group in positioning the substrate with the correct stereoelectronic alignment to enable the nucleophilic attack of the carbonyl carbon by the catalytic cysteine.

Amidases of the nitrilase superfamily, which catalyse the hydrolysis of an amide leading to the formation of carboxylic acid and ammonia play a role in important metabolic processes. For example, hNit2/ω-amidase catalyses the hydrolysis of α-ketoglutaramate (KGM, the α-keto analogue of glutamine) and α-ketosuccinamate (KSM, the α-keto analogue of asparagine), yielding α-ketoglutarate and oxaloacetate, respectively (1,2). Sequence homology within the nitrilase superfamily identifies the cysteine, glutamate (E1), lysine catalytic triad (3,4). The further, structurally-conserved glutamate (E2) is not recognizable from sequence conservation alone as it is located in a loop of variable length, on an exposed surface of the enzyme. The catalytic role of the second glutamate has never been elucidated in detail but it has been shown to be essential for catalysis in the case of the formamidase from *Bacillus cereus* CECT 5050T (5). It has therefore been postulated that the catalytic mechanism of the amidases require four essential amino acid side chains in a precisely conserved geometry (5-8) : a cysteine (C), two glutamates (E1 and E2) and a lysine (K).

The amidase reaction proceeds via a ping-pong bi-bi mechanism involving binding of the amide substrate, the release of ammonia, the formation of a thioester intermediate at the cysteine, the binding of water as the second substrate and finally the release of the carboxylic acid product (9-11). The first crystal structure of a member of the superfamily, a carbamoylase from *Agrobacterium* sp. strain KNK712, led to the proposal that the glutamate (E1) enhances the nucleophilicity of the cysteine enabling it to attack the carbonyl carbon of the amide. The proposal that E1 enhances the nucleophilicity of the cysteine has found wide acceptance in the nitrilase and amidase literature (9,12-14).

The crystal structures of four amidases are known at resolutions below 2 Å. Three are very similar hexamers (PDB IDs 2plq (6), 2uxy (15), and 2dyu (9) while the fourth is a dimer (7)

(PDB ID 3hkx). The structure of the amidase from *Pseudomonas aeruginosa* (PDB ID 2uxy) (15) serendipitously visualizes the tetrahedral intermediate which is formed following the nucleophilic attack by hydroxylamine on the thioester intermediate and thus provides useful mechanistic insights. The structure suggests (a) that the pK_a of the lysine is increased by its interaction with the two active site glutamates (E1 & E2) ensuring that it remains protonated, (b) hydrogen bonds between the substrate carbonyl oxygen and both the lysine and the backbone amide of the residue next in sequence after the cysteine promote the initial attack of the cysteine on the substrate carbonyl carbon and (c) these same interactions stabilize the oxyanion formed on the oxygen of the hydroxamic group of the tetrahedral intermediate (15).

Different roles of the second glutamate (E2) have been suggested during the studies of amidases and D-amino acid carbamoylases. Hung *et al.*(9) noted the role of the residue in the formamidase (AmiF) from *Helicobacter pylori* in maintaining the geometry of the active site and in facilitating the docking of the substrate into the active site. The carbamoylase structures from *Agrobacterium radiobacter* (16) and those deposited by Hashimoto *et al.* (17-20) (PDB IDs 1uf4, 1uf5, 1uf7 and 1uf8), in which a substrate is visualized in complex with an inactive enzyme in which the active site cysteine was substituted by an alanine, shows the amino group of the substrate hydrogen bonded to an oxygen $O^{\varepsilon 2}$ of the E2 carboxylate. A comparable hydrogen bonding arrangement was seen in the C166S mutant of the formamidase from *Helicobacter pylori*, which contained a bound formamide (9). The other carboxylate oxygen $O^{\varepsilon 1}$ of E2 is hydrogen bonded to the ζ-amino group of the active site lysine in most known structures of members of the nitrilase superfamily. Kimani *et al.* (6) suggested a catalytic role for the residue in which it acted as a general base catalyst for the hydrolysis of the thioester intermediate. A role for E2 in the catalysis was confirmed in the case of the formamidase of *Bacillus cereus* CECT (5) by the creation of an inactive mutant in which E2 was replaced by an aspartate. The mutant enzyme was verified to be folded by circular dichroism but the experiments were unable to distinguish whether the loss of activity was due to failure of the aspartate to polarize the lysine of the catalytic triad or whether it failed to act as a general base catalyst.

In this paper we probe the role of E2 by substituting it with a leucine in the amidase from *Geobacillus pallidus* RAPc8 (E142L). No activity is observed with any substrate. A possible consequence of this substitution, consistent with the hypothesis of Kimani *et al*. (6) is that the substrate will react with the cysteine forming the thioester but that this will not be hydrolysed - this would constitute evidence that the residue is acting as a general base catalyst. While no such reaction was observed an alternative outcome was seen in the case of acrylamide - a Michael adduct was formed with the cysteine. Based on the results summarized above this suggests that the inactivity of mutant is due to mispositioning of the substrate thus inhibiting the nucleophilic attack of the cysteine.

EXPERIMENTAL PROCEDURES

Synthesis of E142L mutant -The plasmid used for the expression of the wild-type amidase from *Geobacillus pallidus* RAPc8 (NRRL B-59396) was prepared as described by Cameron *et al*. (21). The glutamate at residue 142 was mutated to a leucine by simple site directed mutagenesis. The mutagenesis was carried out using a pair of overlapping primers (5'- CCT TGG TGT CCG ATC CTC GGA TGG TAT CC - 3' and 5'- GGA TAC CAT CCG AGG CTC GGA CAC CAA GG- 3') and Accuzyme DNA polymerase (Biolione, USA) which has 3'→5' proof reading activity. On completion, the mutagenesis PCR reaction was digested with *Dpn*I restriction enzyme to fragment the methylated template plasmid DNA. E. Cloni (Lucigen, USA) competent cells were transformed with 2 µl of the digested PCR product and the resulting colonies were screened for the mutation by sequencing (Macrogen Inc., Korea). The mutated construct was transformed into *E.coli* BL21 cells (Lucigen, USA) for expression.

Expression and purification of the E142L mutant amidase - The protein was expressed and purified according to the method of Agarkar *et al.* (22) with slight modifications.

Briefly, *E.coli* BL21 cells harbouring the plasmid were grown to logarithmic growth stage in nutrient broth and induced with 1 mM IPTG (Roche, USA) for three hours at 37° C. Cells were then pelleted at 4000 g for 20 min at 4° C and stored at -20 °C overnight. The frozen pellet was thawed on ice and resuspended in 20 mM potassium phosphate buffer, pH7.4, containing 5 mM dithiothreitol (DTT) and protease inhibitor cocktail (Roche, Germany). Sonication was performed on ice using a Misonix 3000 sonicator and the lysate centrifuged at 20 000 g for 30 min at 4° C.

The cell free lysate was then subjected to ammonium sulphate precipitation on ice and the amidase precipitated at 60 and 70% ammonium sulphate saturation as determined by SDS PAGE. The pellets were resuspended in 20 mM potassium phosphate pH 7.4, 5 mM DTT.

These fractions were filtered through a 0.45 µm filter and loaded onto to a HiPrep 16/10 Q-Sepharose FF column (GE Healthcare,USA) equilibrated with 20 mM potassium phosphate pH 7.4, 5 mM DTT, 100 mM NaCl. The proteins were eluted with a linear gradient of 0.1 – 1M NaCl in 20mM potassium phosphate, 2 mM DTT. Fractions containing the amidase were pooled and concentrated in an Amicon ultrafiltration unit using a 10 kDa NMWL polyethersulfone membrane (Millipore, USA) under nitrogen pressure.

The concentrated protein sample was then purified to homogeneity by size exclusion chromatography. It was loaded onto a Sephacryl S-400 gel filtration column (GE Healthcare, USA) equilibrated with 20 mM Tris pH 7.4, 2 mM DTT, 150 mM NaCl. Protein purity was assessed by SDS PAGE and Coomassie blue staining.

Enzyme Activity Assay - Purified wild type amidase and E142L were assayed for activity by a modified indophenol blue assay utilising the Berthelot reaction (23). Briefly, 0.08mg/ml of enzyme was incubated in a 1 mL volume of reaction buffer which consisted of 20 mM potassium phosphate pH 7.4, 150 mM NaCl and 2 mM dithiothreitol. Substrates were added to a final concentration of 10mM. This mixture was incubated at 37° C for 90 min after which ammonia production was detected colorimetrically at 620 nm.

Protein digestion and MALDI Mass spectroscopy - Protein samples were diluted to 1 mg/mL in 90 µL aliquots with 100 mM Tris (Fluka, USA). Substrates were added to the samples at 10-fold molar excess concentration for 30 min before denaturation. To this solution 10 µL of a mixture of 4 M urea (Sigma, USA) and 300 mM dithiotreitol (DTT) was added to a final concentration of 6 M and 30 mM respectively. The protein was denatured for 60 minutes. Proteins were alkylated for 30 min in the dark by adding 30µL of 200 mM iodoacetamide (final concentration 1.5 mM) (Sigma, USA) to the denaturing solution.

The alkylation was stopped by the addition of 30 µL of 300 mM DTT. The digestion mixture was loaded on a 3kD NMW cut-off spin filter (Millipore, Bedford) and 400 µL of 50 mM ammonium bicarbonate pH 8 added. The volume was reduced to 10 µL by centrifugation at 14 000 g for 100 min. The process was repeated twice and the final volume adjusted to 90 µL with 50 mM NH_4HCO_3. Digestion was performed by adding 10 µL of a 0.2 µg/µL trypsin (ABI, Germany) solution. The reaction was terminated by adding trifluoro acetic acid (Sigma, St Louis) to a final concentration of 0.1%. Sample volume was reduced to 10 µL in a SpeedVac vacuum evaporator.

Each sample was fractionated directly onto the MALDI source plate using C_{18} ZipTip® (Millipore, USA) by eluting sequentially with 0.1% TFA/water, 25% ACN/water with 0.1% TFA, 50% ACN/water with 0.1% TFA and 75% ACN/water with 0.1% TFA (ACN GC grade supplied by Brudick and Jackson, USA). The eluted compounds were deposited on the source plate in 3-5µL aliquots. The sample spots were reduced in size by air drying at room temperature before the adding 5 µL of 5 mg/mL α-Cyano-4-hydroxycinnamic acid (Fluka, USA) matrix.

Mass spectral data were acquired on an ABI 4800 MALDI TOF/TOF. Data was acquired in reflectron positive mode with default calibration and the scan range set to *m/z* 800-4000. Spectra were recorded at 50 shots/sub spectrum with a total of 1000 spectra. The source voltage was set to 20 kV with the grid voltage at 16 kV. Delayed extraction time was to

400 ns. Data processing was done with GPS explorer software from ABI.

Protein crystallization and data collection - The purified amidase was crystallized by hanging drop vapour diffusion (22). Briefly, 2 μL of a 10 mg/mL sample of protein was mixed in a 1:1 ratio with the precipitant, 1.2 M sodium citrate, 400 mM sodium chloride and 0.1 M sodium acetate, pH 5.6 and allowed to equilibrate by vapour diffusion. Heavily twinned crystals grew after two days and these were used to streak seed equilibrated drops. Diffraction quality crystals grew after one day at room temperature. Crystals were soaked in the well precipitant solution to which a ten-fold molar excess of amide substrate over protein had been added for at least 24 hr prior to cryo-mounting

These were mounted in nylon loops (Hampton) and vitrified by plunging into liquid nitrogen or in the 100 K nitrogen stream of the cryo-system.

Diffraction data were collected using the diffractometer located on beamline BM 14 at the European Synchrotron Radiation Facility, Grenoble and on a Rigaku diffractometer equipped with a Micromax 007HF copper rotating anode, Varimax HF confocal optical system, AFC 11 Kappa four-circle goniometer, a Saturn 944+ CCD camera and a Cobra cryo-system. Crystals were maintained at 100 K during data collection and diffraction images were collected with either 0.5° or 1° oscillations about a single axis.

Approximately eighty degrees of data were collected for each crystal. In general, only the number of frames necessary to produce a >95% complete dataset were integrated and scaled with d*Trek (24). The structures were solved by rigid body refinement with Refmac5 (25) using the wild-type amidase (6)(PDB ID 2plq) as a model. They were refined by cyclical process involving manual model building with COOT (26) and restrained refinement with Refmac5 (25). In general, no more than two cycles were necessary to achieve convergence as judged by an acceptable fit to the map and the achievement of a minimum value of R_{free} based on 5% of the reflections that were not used in refinement. Analysis of the structures and the molecular graphics diagrams were done with UCSF Chimera (27). The descriptor file for the modified amino acid resulting from the Michael addition of acrylamide to cysteine (S-(3-propanamido)cysteine) was created using Sketcher in the CCP4 package. It is reported in the co-ordinate file as a propionamide (ROP) linked to Cys-166. The co-ordinates were deposited in the PDB with codes 4gyn for the E142L mutant of *Geobacillus pallidus* amidase and 4gyl for the Michael adduct of this mutant enzyme.

Modelling of substrate in the wild type and mutant enzymes - A two–layer combined quantum mechanics and molecular mechanics (QM/MM) ONIOM (28,29) calculation was used to study the structure of the active site in E142L. A Toolkit to Assist ONIOM Calculations (TAO) was used in setting up the calculations from the crystal structure.(30) The high–level (QM) part of the system was calculated using the density functional B3LYP (31-34) with a 6−31+G(d,p) basis set. For the low–level (MM) part the AMBER ff03 force field was used for the enzyme,(35,36) and the generalized AMBER force field (GAFF)(37) with partial charges obtained from a restrained electrostatic potential (RESP)(37-39) fit to the HF/6–31G(d) electron density, for the acrylamide substrate. A mechanical embedding scheme, in which the electrostatic interactions between the high–level and low–level regions are handled through partial atomic charges in the MM Hamiltonian, was used for the geometry optimization. This combined level of theory is commonly denoted ONIOM(B3LYP/6–31+G(d,p):AMBER). The crystal structure of E142L was used as a starting point for the QM/MM calculations, with acrylamide docked in place in the active site, in an orientation consistent with the observed reactivity. The Gaussian 09 package was used for all ONIOM and DFT calculations (40).

RESULTS

1. The enzymatic activity of the E142L mutant amidase - The known substrates of the amidase from *Geobacillus pallidus* RAPc8 are acetamide, acrylamide, lactamide, fluoroacetamide, isobutyramide, formamide and propionamide (41). As demonstrated previously the wild type enzyme was active against all these substrates. However no ammonia was

detected when any of the substrates were incubated with the E142L mutant for 90 min at 37° C in triplicate repeats. The E142L mutation therefore renders the amidase inactive.

2. Mass spectrometry - After reaction with each of the substrates, the E142L mutant amidase was digested with trypsin and the masses of the resulting peptides were determined by mass spectroscopy. In particular an increase in the mass of the peptide which contains the active site cysteine (m/z = 1892) was expected if the predicted thioester intermediate had formed. No changes were observed except in the case of acrylamide (Fig. 1). Relative to the wild type profile there was a decrease in the intensity of the peak at m/z = 1892 and a new peak at m/z = 1963 was observed. This mass shift of +71 is well known to correspond to the formation of a Michael adduct of acrylamide (M_r = 71) to a cysteine. If the thioester intermediate had been formed then a mass shift of +54 would have been measured, corresponding to the mass of acrylamide less the mass of ammonia.

The mass spectrometry experiment was repeated on crystals of the E142L mutant amidase that were soaked in a 10 fold molar excess of acrylamide. The result was similar in that the tryptic fragment containing the active site cysteine was increased in mass by 71 Da relative to the wild-type enzyme. The masses of all other cysteine containing peptides remained the same as they were in the wild-type enzyme.

3. The crystal structures of the E142L mutant of the amidase from Geobacillus pallidus that had been soaked in amide substrates. - Diffraction data were collected from six crystals of the E142L mutant of amidase that had not been exposed to any substrate at the ESRF BM14 beamline. Data from single crystals that had been soaked in one of the substrates: acetamide, isobutyramide, propionamide, fluoracetamide and acrylamide, were collected on the diffractometer with a copper rotating anode source. All the crystals had the same space group symmetry ($P4_232$, with one molecule in the asymmetric unit) and similar unit cell parameters as the wild-type *Geobacillus pallidus* RAPc8 amidase structure (6)(PDB ID 2plq). Data collection and refinement statistics for three crystals are shown in Table 1.

The structure of the E142L amidase mutant shows that the geometry of the active site is maintained (Fig. 2*A*), in particular, the locations of the "catalytic triad": Cys-166, Lys-134 and Glu-59 (E1) are identical to those in the wild-type enzyme (Fig. 2*B*). The leucine side chain of the mutant is slightly displaced from the location of the glutamate in the wild-type enzyme (Fig. 3*A*). There is no significant movement of the backbone atoms in the vicinity of the active site. The leucine side chain is located in poorly defined density suggesting that there are no interactions to constrain its position. Also the loop 139-142 is clearly more mobile as the density in this region, which is well defined in the wild-type enzyme, is broken up and disconnected in some of the mutant crystal structures. This is also shown by the increase in the atomic temperature factors in this region of the model (Fig. 4*A*)

A chloride ion is located 2.9 Å from Lys-134 N^{ζ} and 2.8 Å from the backbone amide nitrogen of Trp-138 (Fig .4*B*). These interactions contribute to the stabilization of the loop and thus, fortuitously, the structural integrity of the mutant enzyme is maintained sufficiently to enable the protein to crystallize. This chloride ion occupies the same position as Glu-142 $O^{\varepsilon 1}$ in the wild-type enzyme. There is no atom in the location of the Glu-142 $O^{\varepsilon 2}$. The Glu-142 $O^{\varepsilon 2}$ equivalent atom is hydrogen bonded to the substrate amino group in the C165A mutant of the carbamylase from *Agrobacterium radiobacter* (16). This same Glu-142 $O^{\varepsilon 2}$ atom forms a hydrogen bond with Tyr-60 O^{η} in the wild-type enzyme but, in spite of the absence of this interaction, the location of Tyr-60 is almost unchanged in the mutant.

There was additional density connected to that of the S^{γ} of Cys-166 in the structure determined from every crystal except those that had been soaked in propionamide and isobutyramide. With the exception of the density seen in the case of the acrylamide soaked crystal, which is discussed in detail below, this density resembled that seen in the wild-type structure described by Kimani *et al*. (6) (Fig. 3C). Essentially, electron density, connected with that of the sulphur extends into the oxyanion hole (42). We interpret this as being due to oxidation of the sulphur in the X-ray

beam. To test this hypothesis we solved the structure of the E142L mutant based on only the first 32 frames and found that this density was substantially reduced (Fig. 3*B*).

In general there was less oxidation in the case of data collected with copper Kα radiation using the 0.3 mm beam produced by the diffractometer optics. In the case of the mutant crystals that had been soaked in propionamide there was no density connected to the S^{γ} but there were two nearby, but separated, spheres of density that were interpreted as water molecules (Fig. 3*A*).

No substrate molecules could be clearly identified in the maps resulting from the crystals soaked in acetamide, isobutyramide, propionamide and fluoracetamide. However the density at Cys-166 in the structure determined from the crystal soaked in acrylamide showed the product of a Michael addition (Fig. 2*B*), thus confirming the mass spectrometry results (Fig. 1). The two water molecules, W1 and W2, that were located in the proximity of Cys-166 were displaced by the Michael adduct. The amide nitrogen was located close to Glu-59 $O^{\varepsilon 2}$ (2.8 Å), Tyr-60 O^{η} (2.8 Å) and the Cl^- (2.8 Å). Both the carbonyl oxygen and Lys-134 N^{ζ} were located in unexpectedly low density below the 2.0 σ contour level possibly because of instability in their positions resulting from their close contact (2.0 Å). The locations of all other atoms in the adduct active site were unchanged (Fig. 3*B*).

4. Modelling the substrate location – An explanation of the docking of the acrylamide substrate leading to the formation of a Michael adduct was sought by modelling using ONIOM, with the substrate and first shell of atoms around the active site being modelled quantum mechanically. In the case of substrate positioned in the wild-type enzyme the distances between the active site atoms and the amide moiety predicted by the ONIOM calculations are comparable to those observed in the deposited crystal structures of two comparable enzymes in which the active site cysteine is mutated to either a serine or an alanine (Table 2). The quantum-mechanical model places the carbonyl oxygen in the oxyanion hole formed by Lys-143 and the backbone amide group of Asp-167 in both the wild-type and the E142L mutant. The amino group, however, instead of being located between the carboxyl oxygens of the two active site glutamates, is drawn towards the chloride ion in the E142L mutant enzyme. This is achieved by pivoting around the carbonyl oxygen, thereby altering the orientation of the amide moiety by more than 60° and bringing the acrylamide C^{β} to within 2.2 Å of the S^{γ} of Cys-166 (Fig. 6).

DISCUSSION

It is clear that Glu-142 plays an essential role in the mechanism of the amidases. Our experiment has helped to define part of this role by demonstrating that, without it, the substrate is mispositioned in the active site. This is illustrated by the successful formation of a Michael's adduct with acrylamide as a result of positioning the double bond close to the active site cysteine and the failure to react in any way with all the other substrates tested. Glu-142 is an essential part of an amide positioning motif also comprising Lys-134, Glu-59 and possibly Tyr-60. It is also clear from our experiment that the hydrogen bond between Glu-142 and Lys-134 assists in stabilizing the loop that contains residues 139 – 142. The other stabilizing interactions that are present, including the chloride ion and the interactions with the adjacent monomer in this hexameric structure were sufficient to ensure structural integrity and enabled the visualizations that we have achieved. Further contributions that Glu142 may make to the chemistry of the active site, such as raising the pK_a of Lys-134, are not addressed by our experiment.

Our initial hypothesis was that Glu-142 acts as a general base catalyst in the second part of the ping-pong bi-bi sequence. That is, it enhances the nucleophilicity of the second substrate, assisting its attack on the carbonyl carbon of the thioester. The second substrate is usually water, but could also be hydroxylamine in the case of an acyl transfer reaction. According to this hypothesis, replacing Glu142 with a leucine would enable the visualization of the thioester intermediate. Mass spectroscopic evidence in the case of the *Rhodococcus* ATCC 39484 nitrilase suggests that either the thioimidate or the thioester forms a stable intermediate in the case of poor nitrile substrates (43). No evidence for the formation of the thioester was found in the case of the amidase

for any of the substrates we tested. Therefore our initial hypothesis was not confirmed directly. It is however not disproved either because of the substantial mispositioning of the substrate in the modified enzyme.

The first part of the reaction, involving a nucleophilic attack by the active site cysteine (Cys-166) on the substrate carbonyl carbon did not occur. Instead the cysteine attacked on the terminal carbon (C^{β}) of the acrylamide. This could only come about as a result of mispositioning the amide moiety so that an attack on the carbonyl carbon was no longer possible. Docking using a QM/MM protocol strengthens this hypothesis and suggests the plausibility of an assisted Michael addition as depicted in Fig. 7. It has frequently been suggested that the nucleophilic attack is assisted by base catalysis involving Glu-59. This could potentially occur in both the occurring formation of the thioester or in the formation of the Michael adduct thus our experiment provides no information concerning this.

Stereoelectronic considerations dictate the trajectory of the nucleophilic attack in the case of the wild-type enzyme. Specifically, the lone pair of the Cys-166 S^{γ} must overlap with the π^* antibonding orbital of the substrate carbon in order to proceed to a stable transition state. Visualization of the details of the state immediately prior to the nucleophilic attack cannot be achieved using X-ray crystallography. The closest approximation that has been achieved involves substitution of an alanine or serine for the active site cysteine. We have not accomplished this for the *G. pallidus* amidase but it has been done for a closely related amidase (9) and carbamoylase (16), enabling us to model the location of the acrylamide in the active site of the wild-type *G. pallidus* amidase.

Our experiment emphasizes the importance of colinear alignment in the transition state of the sulfhydryl p-orbital with that of the amide lowest unoccupied molecular orbital (LUMO) as a prerequisite for the reaction. The models show how the EKE triad together with the backbone atoms, including the peptidic amide of Asp-167 and the peptidic carbonyl of Gly-191 provide a specific amide recognition motif which acts as a vice to position the LUMO. We have shown that without correct substrate positioning brought about inter alia by interactions with Glu-142 $O^{\varepsilon 2}$ the thioester will not form. The study of the catalytic role of Glu-142 in the hydrolysis of the thioester is therefore precluded in the experiment we have performed and it will be necessary to prove the details of its involvement in other ways.

ACKNOWLEDGEMENTS

We thank the Centre for High Performance Computing (CHPC) for use of their resources. The work was funded by grants from the National Research Foundation (NRF) and the Carnegie Corporation of New York. We thank Dr Hassan Belrhali of EMBL, Grenoble for giving us access to the BM14 beamline at ESRF and Professor Wolf-Dieter Schubert for giving us access to the diffractometer at the University of the Western Cape. We thank Dr Mare Vlok for obtaining the mass spectra.

REFERENCES

1. Chien, C. H., Gao, Q. Z., Cooper, A. J. L., Lyu, J. H., and Sheu, S. Y. (2012) Structural insights into the catalytic active site and activity of human Nit2/omega-amidase Kinetic Assay and Molecular Dynamics Simulation. *Journal of Biological Chemistry* **287**, 25715-25726
2. Krasnikov, B. F., Chien, C. H., Nostramo, R., Pinto, J. T., Nieves, E., Callaway, M., Sun, J., Huebner, K., and Cooper, A. J. L. (2009) Identification of the putative tumor suppressor Nit2 as omega-amidase, an enzyme metabolically linked to glutamine and asparagine transamination. *Biochimie* **91**, 1072-1080

3. Bork, P., and Koonin, E. V. (1994) A new family of carbon-nitrogen hydrolases. *Protein Science* **3**, 1344-1346
4. Pace, H. C., and Brenner, C. (2001) The nitrilase superfamily: classification, structure and function. *Genome Biology* **2**
5. Soriano-Maldonado, P., Martinez-Gomez, A. I., Andujar-Sanchez, M., Neira, J. L., Clemente-Jimenez, J. M., Heras-Vazquez, F. J. L., Rodriguez-Vico, F., and Martinez-Rodriguez, S. (2011) Biochemical and mutational studies of the *Bacillus cereus* CECT 5050T formamidase support the existence of a C-E-E-K tetrad in several members of the nitrilase superfamily. *Applied and Environmental Microbiology* **77**, 5761-5769
6. Kimani, S. W., Agarkar, V. B., Cowan, D. A., Sayed, M. F. R., and Sewell, B. T. (2007) Structure of an aliphatic amidase from *Geobacillus pallidus* RAPc8. *Acta Crystallogr. Sect. D-Biol. Crystallogr.* **63**, 1048-1058
7. Nel, A. J. M., Tuffin, I. M., Sewell, B. T., and Cowan, D. A. (2011) Unique aliphatic amidase from a psychrotrophic and haloalkaliphilic *Nesterenkonia* isolate. *Applied and Environmental Microbiology* **77**, 3696-3702
8. Thuku, R. N., Brady, D., Benedik, M. J., and Sewell, B. T. (2009) Microbial nitrilases: versatile, spiral forming, industrial enzymes. *Journal of Applied Microbiology* **106**, 703-727
9. Hung, C. L., Liu, J. H., Chiu, W. C., Huang, S. W., Hwang, J. K., and Wang, W. C. (2007) Crystal structure of *Helicobacter pylori* formamidase AmiF reveals a cysteine-glutamate-lysine catalytic triad. *Journal of Biological Chemistry* **282**, 12220-12229
10. Maestracci, M., Thiery, A., Arnaud, A., and Galzy, P. (1986) A study of the mechanism of the reactions catalyzed by the amidase *Brevibacterium sp.* R312. *Agricultural and Biological Chemistry* **50**, 2237-2241
11. Nakai, T., Hasegawa, T., Yamashita, E., Yamamoto, M., Kumasaka, T., Ueki, T., Nanba, H., Ikenaka, Y., Takahashi, S., Sato, M., and Tsukihara, T. (2000) Crystal structure of N-carbamyl-D-amino acid amidohydrolase with a novel catalytic framework common to amidohydrolases. *Structure with Folding & Design* **8**, 729-737
12. Fernandes, B. C. M., Mateo, C., Kiziak, C., Chmura, A., Wacker, J., van Rantwijk, F., Stolz, A., and Sheldon, R. A. (2006) Nitrile hydratase activity of a recombinant nitrilase. *Advanced Synthesis & Catalysis* **348**, 2597-2603
13. Jandhyala, D. M., Willson, R. C., Sewell, B. T., and Benedik, M. J. (2005) Comparison of cyanide-degrading nitrilases. *Applied Microbiology and Biotechnology* **68**, 327-335
14. Piotrowski, M. (2008) Primary or secondary? Versatile nitrilases in plant metabolism. *Phytochemistry* **69**, 2655-2667
15. Andrade, J., Karmali, A., Carrondo, M. A., and Frazao, C. (2007) Structure of amidase from *Pseudomonas aeruginosa* showing a trapped acyl transfer reaction intermediate state. *Journal of Biological Chemistry* **282**, 19598-19605
16. Chen, C. Y., Chiu, W. C., Liu, J. S., Hsu, W. H., and Wang, W. C. (2003) Structural basis for catalysis and substrate specificity of *Agrobacterium radiobacter* N-carbamoyl-D-amino acid amidohydrolase. *Journal of Biological Chemistry* **278**, 26194-26201
17. Hashimoto, H. A., M.; Shimizu, T.; Nakai, T.; Morikawa, H.; Ikenaka, Y.; Takahashi, S.; Sato, M. . (2003) Crystal structure of C171A/V236A Mutant of N-carbamyl-D-amino acid amidohydrolase. Protein Data Bank

18. Hashimoto, H. A., M.; Shimizu, T.; Nakai, T.; Morikawa, H.; Ikenaka, Y.; Takahashi, S.; Sato, M. . (2003) Crystal structure of C171A/V236A mutant of N-carbamyl-D- amino acid amidohydrolase complexed with N-carbamyl-D-methionine. Protein Data Bank
19. Hashimoto, H. A., M.; Shimizu, T.; Nakai, T.; Morikawa, H.; Ikenaka, Y.; Takahashi, S.; Sato, M. . (2003) Crystal structure of C171A/V236A Mutant of N-carbamyl-D-amino acid amidohydrolase complexed with N-carbamyl-D-valine. Protein Data Bank
20. Hashimoto, H. A., M.; Shimizu, T.; Nakai, T.; Morikawa, H.; Ikenaka, Y.; Takahashi, S.; Sato, M. . (2003) Crystal structure of C171A/V236A Mutant of N-carbamyl-D-amino acid amidohydrolase complexed with N-carbamyl-D-Phenylalanine. Protein Data Bank
21. Cameron, R. A., Sayed, M., and Cowan, D. A. (2005) Molecular analysis of the nitrile catabolism operon of the thermophile *Bacillus pallidus* RApC8. *Biochimica Et Biophysica Acta-General Subjects* **1725**, 35-46
22. Agarkar, V. B., Kimani, S. W., Cowan, D. A., Sayed, M. F. R., and Sewell, B. T. (2006) The quaternary structure of the amidase from *Geobacillus pallidus* RAPc8 is revealed by its crystal packing. *Acta Crystallogr. F-Struct. Biol. Cryst. Commun.* **62**, 1174-1178
23. Horn, D. B., and Squire, C. R. (1966) Estimation of ammonia using indophenol blue reaction. *Clinica Chimica Acta* **14**, 185-&
24. Pflugrath, J. W. (1999) The finer things in X-ray diffraction data collection. *Acta Crystallogr. Sect. D-Biol. Crystallogr.* **55**, 1718-1725
25. Murshudov, G. N., Vagin, A. A., and Dodson, E. J. (1997) Refinement of macromolecular structures by the maximum-likelihood method. *Acta Crystallogr. Sect. D-Biol. Crystallogr.* **53**, 240-255
26. Emsley, P., Lohkamp, B., Scott, W. G., and Cowtan, K. (2010) Features and development of Coot. *Acta Crystallogr. Sect. D-Biol. Crystallogr.* **66**, 486-501
27. Pettersen, E. F., Goddard, T. D., Huang, C. C., Couch, G. S., Greenblatt, D. M., Meng, E. C., and Ferrin, T. E. (2004) UCSF chimera - A visualization system for exploratory research and analysis. *Journal of Computational Chemistry* **25**, 1605-1612
28. Dapprich, S., Komaromi, I., Byun, K. S., Morokuma, K., and Frisch, M. J. (1999) A new ONIOM implementation in Gaussian98. Part I. The calculation of energies, gradients, vibrational frequencies and electric field derivatives. *Journal of Molecular Structure-Theochem* **461**, 1-21
29. Vreven, T., Byun, K. S., Komaromi, I., Dapprich, S., Montgomery, J. A., Morokuma, K., and Frisch, M. J. (2006) Combining quantum mechanics methods with molecular mechanics methods in ONIOM. *Journal of Chemical Theory and Computation* **2**, 815-826
30. Tao, P., and Schlegel, H. B. (2010) Software News and Updates A Toolkit to Assist ONIOM Calculations. *Journal of Computational Chemistry* **31**, 2363-2369
31. Vosko, S. H., Wilk, L., and Nusair, M. (1980) Accurate spin-dependent electron liquid correlation energies for local spin-density calculations - a critical analysis. . *Canadian Journal of Physics* **58**, 1200-1211
32. Becke, A. D. (1993) Density-functional thermochemisty 3. the role of exact exchange. *Journal of Chemical Physics* **98**, 5648-5652
33. Lee, C. T., Yang, W. T., and Parr, R. G. (1988) Development of the Colle-Salvetti correlation-energy formula into a functional of the electron density. *Physical Review B* **37**, 785-789

34. Stephens, P. J., Devlin, F. J., Chabalowski, C. F., and Frisch, M. J. (1994) Ab-initio calculation of vibrational absorption and circular-dichroism spectra using density-functional force-fields. *Journal of Physical Chemistry* **98**, 11623-11627
35. Duan, Y., Wu, C., Chowdhury, S., Lee, M. C., Xiong, G. M., Zhang, W., Yang, R., Cieplak, P., Luo, R., Lee, T., Caldwell, J., Wang, J. M., and Kollman, P. (2003) A point-charge force field for molecular mechanics simulations of proteins based on condensed-phase quantum mechanical calculations. *Journal of Computational Chemistry* **24**, 1999-2012
36. Lee, M. C., and Duan, Y. (2004) Distinguish protein decoys by using a scoring function based on a new AMBER force field, short molecular dynamics simulations, and the generalized born solvent model. *Proteins-Structure Function and Bioinformatics* **55**, 620-634
37. Wang, J. M., Wolf, R. M., Caldwell, J. W., Kollman, P. A., and Case, D. A. (2004) Development and testing of a general amber force field. *Journal of Computational Chemistry* **25**, 1157-1174
38. Bayly, C. I., Cieplak, P., Cornell, W. D., and Kollman, P. A. (1993) A well-behaved electrostatic potential based method using charge restraints for deriving atomic charges - the RESP model. *Journal of Physical Chemistry* **97**, 10269-10280
39. Cornell, W. D., Cieplak, P., Bayly, C. I., and Kollman, P. A. (1993) Application of RESP charges to calculate conformational energies, hydrogen-bond energies and free-energies of solvation. *Journal of the American Chemical Society* **115**, 9620-9631
40. Frisch, M. J., Trucks, G. W., Schlegel, H. B., Scuseria, G. E., Robb, M. A., Cheeseman, J. R., Scalmani, G., Barone, V., Mennucci, B., Petersson, G. A., Nakatsuji, H., Caricato, M., Li, X., Hratchian, H. P., Izmaylov, A. F., Bloino, J., Zheng, G., Sonnenberg, J. L., Hada, M., Ehara, M., Toyota, K., Fukuda, R., Hasegawa, J., Ishida, M., Nakajima, T., Honda, Y., Kitao, O., Nakai, H., Vreven, T., Montgomery, J. A., Jr., Peralta, J. E., Ogliaro, F., Bearpark, M., Heyd, J. J., Brothers, E., Kudin, K. N., Staroverov, V. N., Kobayashi, R., Normand, J., Raghavachari, K., Rendell, A., Burant, J. C., Iyengar, S. S., Tomasi, J., Cossi, M., Rega, N., Millam, J. M., Klene, M., Knox, J. E., Cross, J. B., Bakken, V., Adamo, C., Jaramillo, J., Gomperts, R., Stratmann, R. E., Yazyev, O., Austin, A. J., Cammi, R., Pomelli, C., Ochterski, J. W., Martin, R. L., Morokuma, K., Zakrzewski, V. G., Voth, G. A., Salvador, P., Dannenberg, J. J., Dapprich, S., Daniels, A. D., Farkas, Ö., Foresman, J. B., Ortiz, J. V., Cioslowski J., and Fox, D. J. (2009) Gaussian 09 Revision A. 02. Gaussian Inc., Wallingford CT.
41. Makhongela, H. S., Glowacka, A. E., Agarkar, V. B., Sewell, B. T., Weber, B., Cameron, R. A., Cowan, D. A., and Burton, S. G. (2007) A novel thermostable nitrilase superfamily amidase from *Geobacillus pallidus* showing acyl transfer activity. *Applied Microbiology and Biotechnology* **75**, 801-811
42. Raczynska, J. E., Vorgias, C. E., Antranikian, G., and Rypniewski, W. (2011) Crystallographic analysis of a thermoactive nitrilase. *Journal of Structural Biology* **173**, 294-302
43. Stevenson, D. E., Feng, R., and Storer, A. C. (1990) Detection of covalent enzyme-substrate complexes of nitrilase by ion-spray mass spectroscopy. *Febs Letters* **277**, 112-114

Table 1 Data collection and refinement statistics

	E142L + propionamide (Diffractometer Data)	E142L + acrylamide (Diffractometer data)	E142L (Synchrotron Data, first 32 frames)
PDB code	4gyn	4gyl	Not deposited
Data collection			
X-ray source	Rigaku rotating anode	Rigaku rotating anode	BM14, ESRF
Wavelength (Å)	1.542	1.542	0.9537
Temperature (K)	100	100	100
Space group	$P4_232$	$P4_232$	$P4_232$
Oscillation angle(°)	1	0.5	1
Number of frames	180	200	32
Unit-cell parameter (Å)	a = 130.79	a = 130.49	a = 130.89
Resolution range (Å)	53.39 - 1.90 (1.97 - 1.90)	24.23 - 1.90(1.97 - 1.90)	36.30-1.84
Mosaicity (°)	0.22	0.23	1.10
No. of observed reflections	164555	486668	221828
No. of unique reflections	29066	30455	33703
No. of unique reflections in test set	1446	1533	1654
Completeness (%)	94.6 (93.7)	99.9 (99.1)	99.7 (99.5)
Multiplicity	5.66 (5.09)	15.98 (6.56)	6.58 (4.87)
$\langle I/\sigma(I)\rangle$	5.0 (2.3)	7.8 (2.1)	10.6 (2.8)
Wilson B factor ($Å^2$)	24.9	28.3	29.5
R_{merge}‡	0.205 (0.464)	0.246 (0.635)	0.080 (0.470)
R_{meas}†	0.225 (0.516)	0.253 (0.688)	0.087 (0.526)
No. of protein molecules in asymmetric unit	1	1	1
Matthews coefficient, V_M ($Å^3$ Da^{-1})	2.5	2.5	2.5
Solvent content (%)	50	50	50

Refinement			
Resolution range (Å)	53.39-1.90	24.23 - 1.90	36.30-1.84
Contents of asymmetric unit (excluding hydrogen atoms):			
No. of protein atoms	2661	2659	2661
No. of chloride ions	1	1	1
No. of water atoms	213	243	205
Average B factor ($Å^2$)	14.5	17.5	28.7
R.m.s. deviations from ideal			
Bond lengths (Å)	0.019	0.022	0.28
Bond angles (°)	1.41	2.08	2.28
Ramachandran favoured	319	319	317
Ramachandran allowed	16	16	15
Ramachandran outliers	3	3	3
R_{cryst}§	0.17 (0.23)	0.17 (0.19)	0.20
R_{free}¶	0.20 (0.27)	0.19 (0.21)	0.22

Table 2

Mean distances between the substrate amide N, C and O atoms and the key active site residues (Glu-1, Glu-2, Lys and Cys). The backbone NH is that of the residue immediately following the active site cysteine.

	C166S mutant of AmiF from *Helicobacter pylori* (Å)	C171A mutant of the carbamoylase from *Agrobacterium* sp.(Å)	ONIOM model of acrylamide bound to the wild-type amidase (Å)	ONIOM model of acrylamide bound to the E142L mutant amidase (Å)
N…Glu-1 $O^{\varepsilon 2}$	2.9	3.0	2.8	3.6
N…Glu-2 $O^{\varepsilon 2}$	3.1	3.4	3.0	N/A
N…Cl^-	N/A	N/A	N/A	3.0
C…Cys C^{β}	3.5	3.4	3.6	3.6
C…Cys S^{γ}	N/A	N/A	3.1	3.2
O…Lys N^{ζ}	3.3	2.8	2.7	2.6
O…NH	3.1	3.2	3.2	3.2

FIGURE LEGENDS

FIGURE 1. **Identification of adduct formation.** Part of the mass spectrum of the tryptic digest of the E142L mutant of the amidase from *G. pallidus*. (A) Shows the peak corresponding the tryptic fragment containing the active site cysteine, Cys 166. (B) Shows the 71 Da mass shift in this fragment after reaction with acrylamide. No other cysteine containing fragments experienced a mass shift after the reaction.

FIGURE 2. **The active site of the E142L mutant.** (A) Electron density map of the E142L mutant of the amidase from *Geobacillus pallidus* RAPc8 contoured at 1.0 σ . Three distinct spheres of density in the active site are interpreted as a chloride ion and two water molecules. The chloride ion is 2.9 Å from the amino group nitrogen of lysine 134 and 2.9 Å from the backbone amino group of tryptophan 138 (labelled 138). (B) The electron density map of the corresponding volume of the product of the reaction of the amidase with acrylamide. A Michael adduct is formed with cysteine 166. The amide nitrogen of the adduct is located 2.9Å from the chloride which, in turn, moves slightly further away from the mean position of the Lys-134 N^{ζ} (3.1 Å). There is a close contact between the lysine 134 N^{ζ} and the carbonyl oxygen of the adduct resulting in both atoms having lower than expected electron densities. The distance between the mean locations of these two atoms is 2.1 Å.

FIGURE 3. **A comparison of the active site of the the wild type enzyme with the E142L mutant .** A, An overlay of the active site residues of the wild-type and mutant (E142L) amidase enzymes . The geometry of the common active site residues, Cys 166, Lys 134, Glu59 and Tyr 60 are maintained. A chloride ion in the E142L mutant occupies the same position as the Glu142 $O^{\varepsilon 1}$ in the wild-type enzyme. The position of Leu 142 is displaced from the position originally occupied by Glu 142. B shows an overlay of the E142L mutant amidase before and after reaction with acrylamide. The amide oxygen of the Michael adduct at Cys166 after incubation with acrylamide is in close contact with Lys-134. The two water molecules, W1 and W2, are displaced by the adduct.

FIGURE 4. **Stabilization of loop 139 – 143.** A, A superposition of residues in the loop 139-143 from the wild type enzyme and the E142L mutant enzyme coloured according to atomic temperature factors in UCSF Chimera. In the wild-type amidase the position of the loop is constrained by the interactions of Glu-142 with Lys-134 and Tyr-60 and has low temperature factors. In the E142L mutant enzyme these constraint are absent and thus the loop is more flexible as evidenced by the increased temperature factors. The rendering of the temperature factors utilises a continuous colour spectrum in which dark blue has a value of 3 $Å^2$, green 18 $Å^2$ and a red 35 $Å^2$. B, In the E142L mutant some stabilization of the loop is achieved through interactions with the chloride ion. The chloride ion is positioned 2.8 Å from the backbone amide nitrogen of Trp-138 and 2.9 Å from Lys-134 N^{ζ}.

FIGURE 5. **Cysteine oxidation.** The electron density shown at 0.6 σ surrounding Cys-166 in: A, the map obtained using data collected from a crystal of the E142L mutant of the amidase which had been soaked in propionamide (PDB ID 4gyn), B, the map obtained using the first 32 frames of data collected from a crystal of the E142L mutant of the amidase (Table 1, column 3) and C, the map obtained from a crystal wild-type amidase (PDB ID 2plq). The oxygens of the water molecules W1 and W2 depicted in A are located as follows: W1, 3.2Å from Cys-166 S^{γ} and 2.7 Å from the backbone carbonyl oxygen of Gly-191 and W2, 2.9 Å from Lys-134 N^{ζ} and 2.8 Å from Tyr-60 O^{η}. W2 is 4.0 Å from Cys-166 S^{γ}.

FIGURE 6. **Acrylamide docking using ONIOM.** The formation of the Michael adduct in the E142L mutant enzyme is explained by QM/MM modelling of the acrylamide in the active site pocket of the wild-type enzyme, depicted with magenta carbon atoms, superimposed on the mutant depicted with grey carbon atoms. In the mutant enzyme the acrylamide pivots around the carbonyl oxygen, which is located in the oxyanion hole formed by Lys-134 and the backbone amide of Asp-167 (labelled167), as the amino group is drawn towards the chloride ion. In this conformation the acrylamide C^{β} is positioned close to the S^{γ} of Cys-166 and the stereo electronic alignment, which is essential for the nucleophilic attack on the carbonyl carbon, is lost.

FIGURE 7. **Proposed reaction scheme for the formation of the Michael adduct.** The nucleophilic sulphur of Cys-166 of the E142L mutant attacks the acrylamide at the terminal or β-carbon instead of the carbonyl carbon due to the mispositioning of the amide group in the active site. The positive charge of Lys-134 transiently stabilises the enolate intermediate which subsequently collapses, resulting in the formation of a stable Michael adduct at Cys-166. Our experiment does not provide insight into which base transiently binds the proton, but it could possibly be Glu-59.

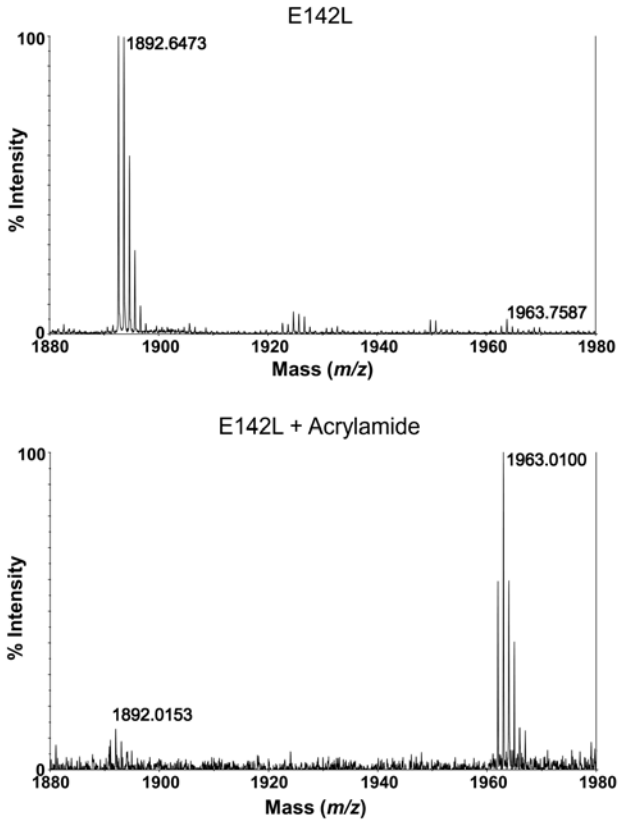
E142L
100
1892.6473
% Intensity
0
1963.7587
1880
1900
1920
1940
1960
1980
Mass (m/z)
E142L + Acrylamide
100
1963.0100
% Intensity
1892.0153
0
1880
1900
1920
1940
1960
1980
Mass (m/z)

Figure 1

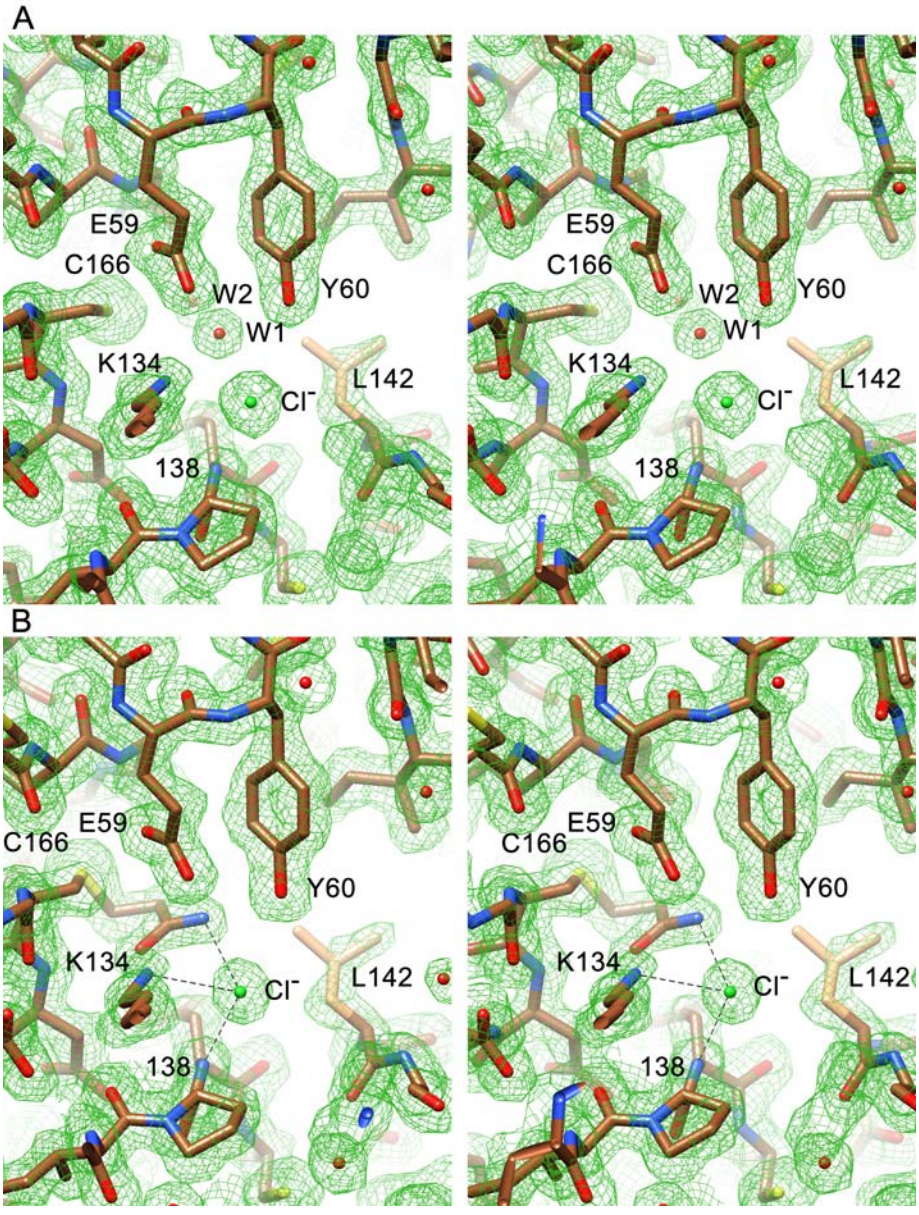
A
E59
C166
W2
Y60
W1
K134
Cl-
L142
138
B
C166
E59
Y60
K134
Cl-
L142
138

Figure 2

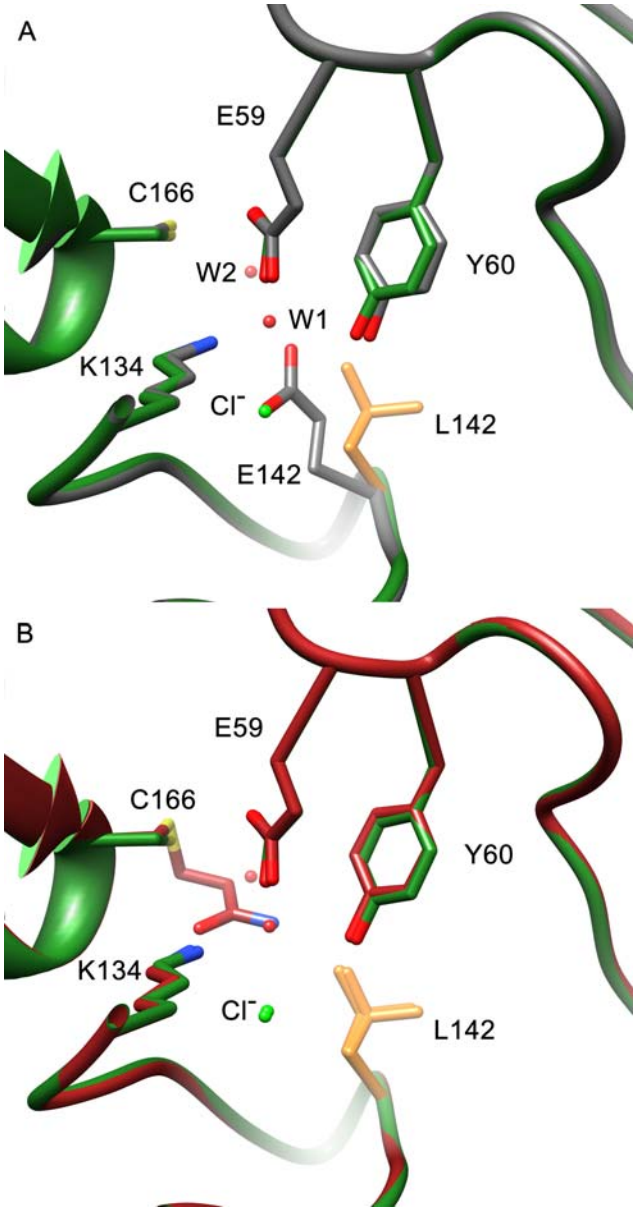
A
E59
C166
W2
Y60
W1
K134
Cl⁻
L142
E142
B
E59
C166
Y60
K134
Cl⁻
L142

Figure 3

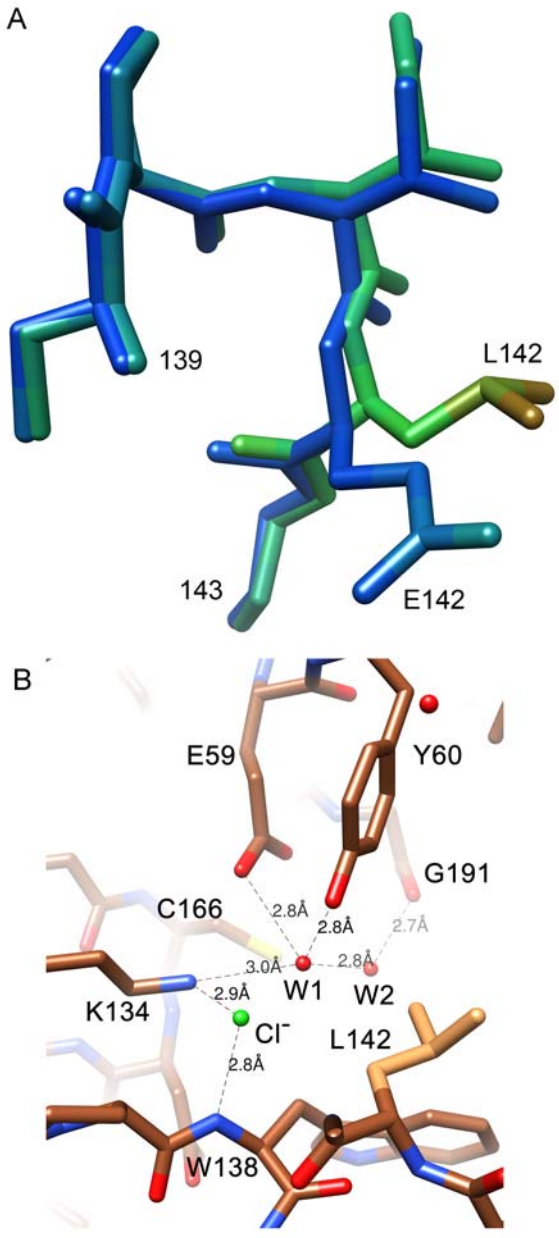
A
139
L142
143
E142
B
E59
Y60
G191
C166
2.8Å
2.8Å
2.7Å
3.0Å
2.8Å
2.9Å
W1
W2
K134
Cl⁻
L142
2.8Å
W138

Figure 4

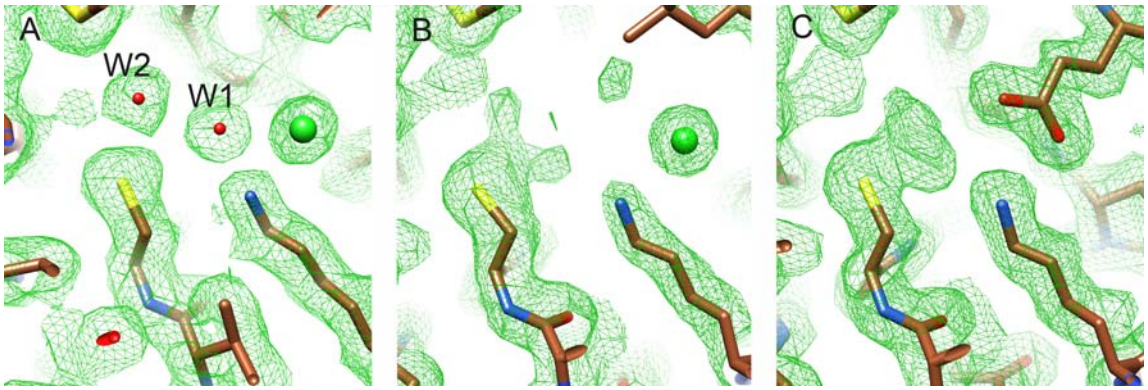

Figure 5

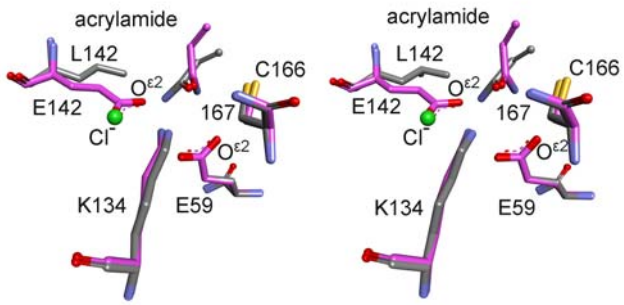
acrylamide
L142
Oε2
E142
Cl-
C166
167
Oε2
K134
E59
acrylamide
L142
Oε2
E142
Cl-
C166
167
Oε2
K134
E59

Figure 6

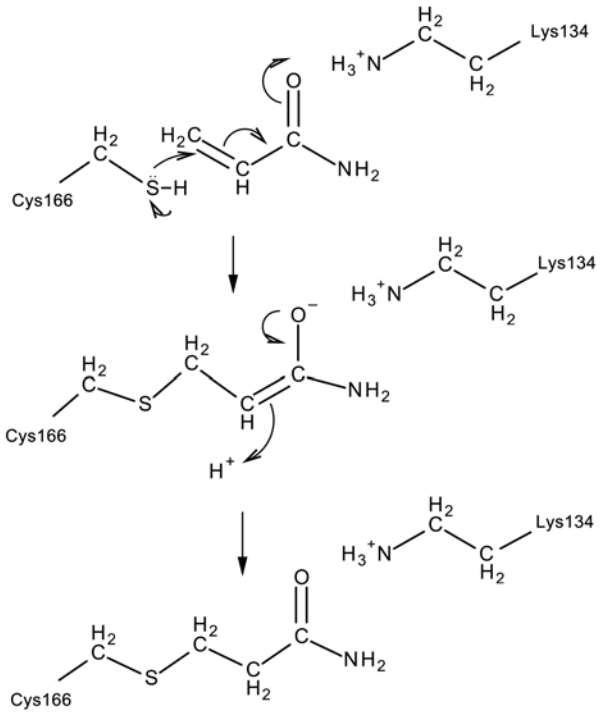

Figure 7